Dual Low-Rank Adaptation for Continual Learning with Pre-Trained Models

Huancheng Chen
University of Texas at Austin
huanchengch@utexas.edu

Jingtao Li
SonyAI
jingtao.li@sony.com

Nidham Gazagnadou
SonyAI
nidham.gazagnadou@sony.com

Weiming Zhuang
SonyAI
wingalong@gmail.com

Chen Chen
SonyAI
ChenA.Chen@sony.com

Lingjuan Lyu*
SonyAI
lingjuan.lv@sony.com

Abstract

In the era of foundation models, we revisit continual learning (CL), which aims to enable vision transformers (ViTs) to learn new tasks over time. However, as the scale of these models increases, catastrophic forgetting remains a persistent challenge, particularly in the presence of significant domain shifts across tasks. Recent studies highlight a crossover between CL techniques and parameter-efficient fine-tuning (PEFT), which focuses on fine-tuning only a small set of trainable parameters to adapt to downstream tasks, such as low-rank adaptation (LoRA). While LoRA achieves faster convergence and requires fewer trainable parameters, it has seldom been explored in the context of continual learning. To address this gap, we propose a novel PEFT-CL method called Dual Low-Rank Adaptation (DualLoRA), which introduces both an orthogonal LoRA adapter and a residual LoRA adapter parallel to pre-trained weights in each layer. These components are orchestrated by a dynamic memory mechanism to strike a balance between stability and plasticity. The orthogonal LoRA adapter's parameters are updated in an orthogonal subspace of previous tasks to mitigate catastrophic forgetting, while the residual LoRA adapter's parameters are updated in the residual subspace spanned by task-specific bases without interaction across tasks, offering complementary capabilities for fine-tuning new tasks. On ViT-based models, we demonstrate that DualLoRA offers significant advantages in accuracy, inference speed, and memory efficiency over existing CL methods across multiple benchmarks.

1. Introduction

Continual learning (CL) [25], which involves training a model on a sequence of tasks, often faces the challenge of *catastrophic forgetting*—a significant degradation in performance on previous learned tasks when learning new ones.

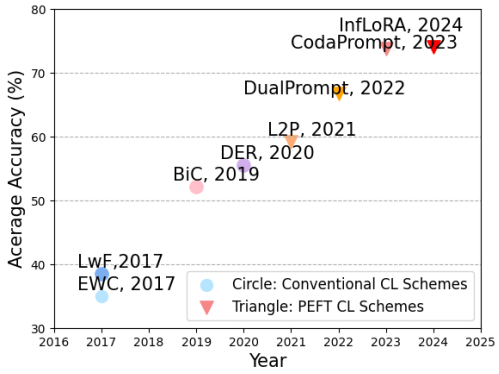

Figure 1. PEFT-CL schemes dominate the ImageNet-R dataset.

This problem persists in the context of continuously training of vision foundation models, despite their renowned generalization capabilities and robustness. The existing replay-based CL schemes [1, 2, 31] typically mitigate forgetting by storing a subset of data from previous tasks as *exemplars*, but this approach can be challenging in practice due to data retention policies. On another note, architecture-based CL schemes [15, 19, 20] allocate isolated parameters for each task associated with a task identifier during training for preventing interference across tasks. Nevertheless, vision foundation models risk losing their pre-trained capabilities if their architecture is modified for fine-tuning on downstream tasks, as the pre-trained weights are learned in the predetermined architecture. Additionally, these methods often assume that task identity is known during inference, which is unrealistic in real-world scenarios.

Recently, parameter-efficient fine-tuning (PEFT) techniques [8, 14] have attracted significant attention due to their capacity to adapt foundation models to downstream tasks by updating or adding only a small number of parameters. Furthermore, PEFT methods have demonstrated notable robustness in mitigating catastrophic forgetting when

applied to sequential task fine-tuning. In particular, prompt-tuning [24, 27–29] and low-rank adaptation (LoRA) [17, 30] are two widely-used PEFT approaches that have shown remarkable success in the context of continual learning, significantly outperforming conventional CL schemes across established benchmarks (Fig. 1). As illustrated in Fig. 2.a, prompt-tuning methods mainly focus on learning a *prompt pool* that enables matching an image with a set of prompt vectors and aligning features of the image along with the patch tokens. However, the aforementioned prompt-based CL methods require using the original pre-trained encoder as the query function. This results in the image tokens being processed through the network **twice**, leading to significant computational overhead and increased inference latency.

In contrast, LoRA methods require fewer trainable parameters to achieve comparable performance on domain-specific tasks and enable faster inference speeds compared to prompt-tuning. Nevertheless, the vanilla LoRA [8] struggles to preserve satisfactory performance in continual learning settings due to significant interference across different tasks. Inspired by the idea of gradient projection [5, 23], InfLoRA [17] take the first step to mitigate such interference by initializing LoRA adapter parameters for new tasks within a subspace orthogonal to the gradient subspace derived from previously learned tasks. However, InfLoRA involves **twice** pass through the encoder for each sample in a task: the first pass extracts the gradient subspace for LoRA initialization (as depicted in Fig. 2.b), and the second pass updates the parameters, resulting in substantial computational overhead.

To this end, we propose a novel continual learning method, dual low-rank adaptation (DualLoRA), which incorporates an orthogonal adapter and a residual adapter in each layer of pre-trained vision transformers (ViTs). Specifically, the orthogonal adapter $\mathbf{O}$ is exclusively updated in directions orthogonal to features extracted from previously learned tasks, while the residual adapter $\mathbf{R}$ is updated in task-specific subspace spanned by the residual bases extracted by the last learn task. This design aims to enhance *stability*, *i.e*. robustness to forgetting on old tasks, with orthogonal adapters while increasing *plasticity*, *i.e*. the ability to adapt to new tasks continuously, with residual adapters, thereby striking a balance between both objectives.Unlike InfLoRA, DualLoRA efficiently extracts core bases of the feature subspace from previously learned tasks and projects the updates of $\mathbf{O}$ and $\mathbf{R}$ using matrices constructed from these extracted bases. Moreover, these bases can be employed to compute task relevance during inference, enabling the residual adapter's outputs to be adjusted based on task relevance to mitigate components that could degrade test performance. This mechanism, which dynamically modulates the parameters of the residual adapter according to input test samples during inference, is referred to as *dynamic memory* (DM), as illustrated in Fig. 2.c. The task relevance obtained from test samples not only refines the feature embeddings but also enhances task identity prediction, which has shown significant benefits in continual learning within this work. Extensive experimental results demonstrate that DualLoRA outperforms existing PEFT methods across various continual learning benchmarks, without incurring significant additional computational or memory overhead. The main contributions of this paper are summarized as follows:

- We introduce a novel low-rank adaptation paradigm for fine-tuning ViTs in continual learning settings. This paradigm efficiently extracts feature subspaces from previously learned tasks using singular value decomposition and mitigates catastrophic forgetting by reducing task interference through gradient projection.
- To address the challenge of limited update space due to gradient projection, we design a dual LoRA structure consisting of an orthogonal adapter and a residual adapter. This design integrates the proposed dynamic memory mechanism, effectively balancing stability and plasticity in continual learning.
- To further improve the performance of DualLoRA, we develop a simple and efficient method for inferring task identities of test samples during inference, leveraging the extracted feature subspaces. Extensive experimental results demonstrate the superior performance of DualLoRA compared to state-of-the-art baselines.

2. Background and Related Work

2.1. Gradient Projection in Continual Learning

Gradient projection is widely employed in continual learning to mitigate catastrophic forgetting by updating parameters in directions that minimize interference with previously learned tasks. OGD [5] firstly implements gradient descent in the orthogonal direction to stored gradient directions computed in the previous tasks. In contrast, the concurrent work GPM [23] extracts core bases of the task representations from randomly selected training data via singular value decomposition (SVD). A subsequent study, TRGP [18], introduces the concept of a trust region, allowing partial reuse of selected bases from previous tasks. FSDGPM [3] further evaluates the importance of bases in GPM by assessing the sharpness of the loss landscape, assigning weights to the bases in the projection matrix according to their relative importance. Due to the computational expense of determining loss landscape sharpness, SGP [22] offers an alternative by using accumulated singular values as an importance indicator to scale the projection matrix in GPM. Additionally, several studies [11, 16, 26, 32] have explored relaxing the orthogonality constraints and optimizing the relaxation factor to enhance performance. However,

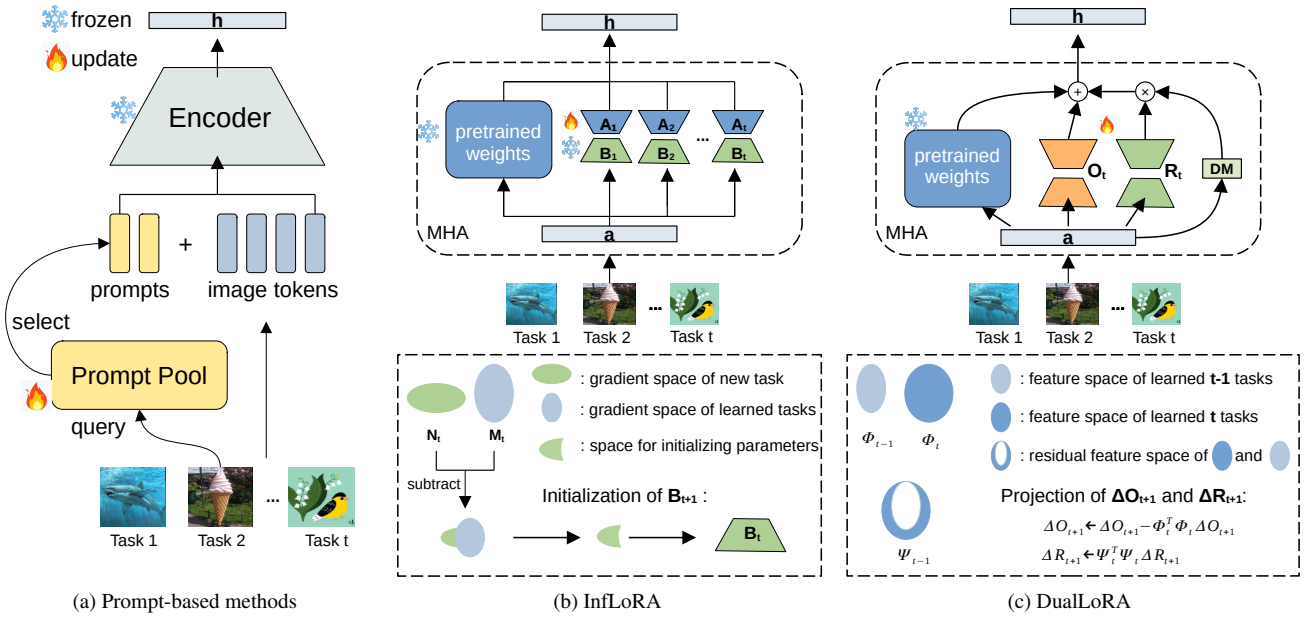

(a) Prompt-based methods (b) InfLoRA (c) DualLoRA

Figure 2. Comparison of the proposed (c) DualLoRA paradigm with (a) prompt-based schemes (L2P [29], DualPrompt [28], CodaPrompt [24]) and (b) InfLoRA [17]. Both prompt-based methods and InfLoRA require to forward each sample in the training dataset **twice**.

these approaches are primarily developed for simpler models such as CNNs and face significant challenges when applied to advanced architectures like ViTs. For instance, the high dimensionality of feature embeddings in ViTs leads to substantial computational overhead when performing SVD. This motivates us to explore more efficient methods for extracting core bases from feature subspaces in ViTs.

2.2. Parameter-Efficient Fine-Tuning in CL

Parameter-efficient fine-tuning (PEFT) methods enable adapting pre-trained models to downstream tasks by fine-tuning only a small number of trainable parameters. Among these, prompt-tuning [14] has demonstrated strong robustness in learning sequential tasks and has achieved remarkable success in continual learning benchmarks, significantly outperforming traditional continual learning schemes. The pioneering work L2P [29] addresses continual learning challenges by introducing a prompt pool that matches top-k relevant queries, serving as supplementary input to facilitate feature alignment in the pre-trained model. The follow-up study, DualPrompt [28] takes a step further by employing task-invariant *G-Prompts* and task-specific *E-Prompts* to capture both shared and task-specific knowledge across different tasks. S-Prompt [27] independently learns prompts across domains, using K-means clustering on features of training data and a K-NN algorithm to match test data with domain-specific prompts. CodaPrompt [24] shifts the focus from fixed instance-specific prompts to a set of prompt components, selecting a weighted combination of these components for each instance based on attention scores.

Despite the remarkable success of prompt-tuning methods in continual learning, these approaches require both training and testing data to be passed through the query function (typically the original pre-trained model) for feature extraction before fine-tuning and inference, resulting in longer fine-tuning and inference times. Recently, PGP [21] has adapted the gradient projection approach from GPM to prompt-tuning, aiming to mitigate forgetting by applying orthogonal projection to the gradients of the prompt pool, though it inherits the limitations of prompt-tuning. Similarly, InfLoRA [17] marks the first attempt to apply gradient projection in low-rank adaptation for ViT models [4], storing gradient directions from learned tasks during fine-tuning. However, InfLoRA introduces significant computational overhead due to performing singular value decomposition (SVD) on the high-dimensional gradient subspace, which is computationally more expensive than the original LoRA. Moreover, the core bases derived from the gradient subspace cannot be utilized to infer task identities during inference, as gradients are not available at that stage. This challenge motivates us to explore the use of gradient projection based on the core bases in the feature subspace, enabling the modulation of dynamic memory during inference for improving average test performance.

3. Preliminary

3.1. Continual Learning Problem Setting

Given a pre-trained model with backbone parameters $\mathbf{W}_0$, we aim to fine-tune the model by adding adapters $\mathcal{A}_l$ in the

l-th layer of the model and the classifier $\mathcal{F}$ to fit a sequence of domain data $\mathcal{D}_t = \{\mathbf{x}_i, \mathbf{y}_i\}_{i=1}^{|\mathcal{D}_t|}$, where $\mathbf{x}_i$ denotes data samples and $\mathbf{y}_i \in \mathcal{Y}_t$ denotes corresponding labels in the t-th task. In the challenging class-incremental setting, there is no intersection between the label sets from two different tasks as $\mathcal{Y}_{t_1} \cap \mathcal{Y}_{t_2} = \emptyset$ for all $t_1 \neq t_2$. When learning a new task, access to the old task data becomes unavailable due to storage constraints. The objective function in continual learning is to minimize the empirical risk of the unified adapters $\mathcal{A}_{1:L}$ integrated in L layers of the pre-trained model that performs inference on the sequence of data from T various tasks as follow:

$$\min_{\{\mathcal{A}_l\}_{l=1}^{L}, \mathcal{F}} \frac{1}{T} \sum_{t=1}^{T} \mathcal{L}_{\text{task}}(\mathbf{W}_0, \mathcal{A}_{1:L}, \mathcal{F}, \mathcal{D}_t), \tag{1}$$

where $\mathbf{W}_0$ is the frozen backbone parameters of the pre-trained model; $\mathcal{L}_{\text{task}}(\cdot)$ is the loss function depending on the specific task. The classifier $\mathcal{F}$ consists of an expanding set of fully-connected layers $f_t : \mathbb{R}^d \to \mathbb{R}^{C_t}$, where d is the dimension of embedding and C_t is the number of classes in the t-th task. Given **no task identities** during inference, all the learned $f_t(\cdot)$ are used to predict categories of input data.

3.2. Multi-Head Attention Block

Vision transformer (ViT) models [4] break down images into n patches and flatten these patches into patch embeddings with dimension d. The encoder of a ViT consists of a sequence of multi-head attention (MHA) blocks containing *key*, *query* and *value* weights $\mathbf{W}^q, \mathbf{W}^k$ and $\mathbf{W}^v$ for mapping input activation signals $\mathbf{a}^{(l)}$ into $\mathbf{Q}^{(l)}$, $\mathbf{K}^{(l)}$ and $\mathbf{V}^{(l)}$ and obtaining the output signals $\mathbf{h}^{(l)}$ by computing

$$\mathbf{h}^{(l)} = \text{softmax}\left(\frac{\mathbf{Q}^{(l)}\left(\mathbf{K}^{(l)}\right)^T}{\sqrt{d}}\right) \cdot \mathbf{V}^{(l)}, \tag{2}$$

where $\mathbf{Q}^{(l)} := \mathbf{a}^{(l)}\mathbf{W}^q$, $\mathbf{K}^{(l)} := \mathbf{a}^{(l)}\mathbf{W}^k$ and $\mathbf{V}^{(l)} := \mathbf{a}^{(l)}\mathbf{W}^v$. The output signals $\mathbf{h}^{(l)}$ undergo normalization and are then forwarded to the next MHA block until $\mathbf{h}^{(L)}$ is directed to the classifier.

3.3. Low-Rank Adaptation

Low-rank adaptation (LoRA) [8] is a parameter-efficient fine-tuning method that enables reducing memory consumption by assigning learnable rank decomposition matrices $\mathbf{A} \in \mathbb{R}^{r\times d}$ and $\mathbf{B} \in \mathbb{R}^{d\times r}$ parallel to the frozen pre-trained weights $\mathbf{W}_0 \in \mathbb{R}^{d\times d}$ into each layer of the model as follow,

$$\mathbf{W} := \mathbf{W}_0 + \mathbf{BA}, \tag{3}$$

where $\mathbf{W}$ denotes model weights after fine-tuning, and $r \ll d$. In this paper, we follow the strategy in [6], and only implement LoRA fine-tuning on $\mathbf{W}_0^k$ and $\mathbf{W}_0^v$ while keeping $\mathbf{W}_0^q$ frozen during the whole procedure.

4. Methodology: Dual Low-Rank Adaptation

As gradients are projected onto subspaces orthogonal to the feature subspaces of previously learned tasks, the space available for model updates becomes increasingly constrained. To address this, several studies [3, 18, 32] have relaxed the strict orthogonality constraints to expand the optimization subspace for new tasks, accounting for the stability-plasticity trade-off. Building on these insights, we propose a novel low-rank adaptation framework, DualLoRA, which comprises an orthogonal adapter $\mathbf{O} := \mathbf{A}_o\mathbf{B}_o \in \mathbb{R}^{d\times d}$ and a residual adapter $\mathbf{R} := \mathbf{A}_r\mathbf{B}_r \in \mathbb{R}^{d\times d}$, updated in the orthogonal and residual directions, respectively, as depicted in Fig. 2.c. In the subsequent sections, we will detail the process of updating both adapters and describe how dynamic memory is integrated during model inference.

4.1. Orthogonal Adapter

The concept of using orthogonal gradient projection to mitigate forgetting originated from GPM [23], which involves flattening feature maps extracted by convolutional kernels into vectors and performing singular value decomposition (SVD) on these vectors to obtain core feature bases. However, vectorizing the patch embedding of a ViT with dimensions (n, d) necessitates extensive computation in SVD, particularly when dealing with high-resolution inputs. n vision transformers, feature embeddings are often redundant for classification tasks, as only the first embedding (commonly referred to as the *class token*) is passed to the classifier for prediction.

To this end, we propose an efficient method for extracting the core bases of the class-token subspace without performing SVD on the entire high-dimensional embedding space. Specifically, given the pre-trained weights $\mathbf{W}_0^q$, $\mathbf{W}_0^k$, and $\mathbf{W}_0^v$, the fine-tuned *key* and *value* weights $\mathbf{W}_{t+1}^k$ and $\mathbf{W}_{t+1}^v$ for the $(t+1)$-th task can be derived as follows:

$$\mathbf{W}_{t+1}^i = \mathbf{W}_0^i + \sum_{\tau=1}^{t+1} \Delta\mathbf{O}_\tau^i = \mathbf{W}_t^i + \Delta\mathbf{O}_{t+1}^i, \quad \forall i \in \{k, v\}, \tag{4}$$

where $\Delta\mathbf{O}_\tau^i$ is the update of the orthogonal adapter computed from the τ-th task. According to (2), when we fine-tune the parameters on the $(t+1)$-th task, the change of output signal $\mathbf{h}^{(l)}$ given the same data can be found as

$$\begin{aligned}\Delta\mathbf{h}^{(l)} = \Gamma \cdot \frac{\mathbf{Q}^{(l)}\left(\mathbf{a}^{(l)}\Delta\mathbf{O}_{t+1}^k\right)^T}{\sqrt{d}} \cdot \mathbf{V}^{(l)} \\ + \underbrace{\text{softmax}\left(\frac{\mathbf{Q}^{(l)}\left(\mathbf{K}^{(l)}\right)^T}{\sqrt{d}}\right) \cdot \mathbf{a}^{(l)}}_{\mathbf{S}^{(l)}} \Delta\mathbf{O}_{t+1}^v,\end{aligned} \tag{5}$$

where Γ is a diagonal matrix (the derivation is deferred to

Appendix 1). To preserve the value of class-token in $\mathbf{h}^{(L)}$ output by the last layer, we must guarantee $\Delta\mathbf{h}_1^{(l)} = \mathbf{0}$ for each layer so the class-token of the same test sample from old tasks can be preserved after fine-tuning on the new task. Since $\mathbf{Q}^{(l)}$ is unchanged with the frozen weight $\mathbf{W}_0^q$, we need to project $\left(\Delta\mathbf{O}_{t+1}^k\right)^T$ into the subspace orthogonal to the core bases of $\mathbf{k}^{(l)} := \mathbf{Q}_1^{(l)}$, denoting the first row of $\mathbf{Q}^{(l)}$. Meanwhile, $\Delta\mathbf{O}_{t+1}^v$ must be orthogonal to the bases of $\mathbf{v}^{(l)} := \mathbf{S}_1^{(l)}$, the first row of $\mathbf{S}^{(l)}$. Following the strategy in GPM [23], we randomly sample m data points from the current task after fine-tuning on the t-th task and input these m samples to the model for obtaining embedding matrices $\tilde{\mathbf{K}}^{(l)} \in \mathbb{R}^{m\times d}$ consisting of $\{\mathbf{k}_i^{(l)}\}_{i=1}^m$ and $\tilde{\mathbf{V}}^{(l)} \in \mathbb{R}^{m\times d}$ consisting of $\{\mathbf{v}_i^{(l)}\}_{i=1}^m$. We update the new feature matrices $\mathbf{\Phi}_t^k$ and $\mathbf{\Phi}_t^v$ by extracting the core bases of $\tilde{\mathbf{K}}^{(l)}$ and $\tilde{\mathbf{V}}^{(l)}$ using SVD and concatenating them into the previous feature matrices $\mathbf{\Phi}_{t-1}^k$ and $\mathbf{\Phi}_{t-1}^v$. With the feature matrices obtained on the t-th task, we can project the updates $\Delta\mathbf{O}_{t+1}^k$ and $\Delta\mathbf{O}_{t+1}^v$ by

$$\Delta\mathbf{O}_{t+1}^i \leftarrow \Delta\mathbf{O}_{t+1}^i - (\mathbf{\Phi}_t^i)^T\mathbf{\Phi}_t^i\Delta\mathbf{O}_{t+1}^i, \quad \forall i \in \{k, v\}. \tag{6}$$

When we select m data points, with $m \ll d$, for extracting core bases, the complexity of SVD is $\mathcal{O}(m^2d)$, which is much more efficient than implemented SVD with $\mathcal{O}(d^3)$ in the previous work InfLoRA [17]. We emphasize that our orthogonal adapters undergo a different update process than InfLoRA, where core bases are extracted from the gradient subspace. Instead, we develop an alternative feature set, $\mathbf{S}^{(l)}$, specifically to preserve the class token, as outlined in Eq. 5. This approach enables a more efficient SVD, providing a lightweight solution in comparison to the original GPM method.

4.2. Residual Adapter

As the feature subspaces represented by $\mathbf{\Phi}_t^k$ and $\mathbf{\Phi}_{t+1}^v$ expand with the accumulation of learned tasks, the majority of the components in the updates, $\Delta\mathbf{O}_{t+1}^k$ and $\Delta\mathbf{O}_{t+1}^v$, are progressively subtracted, as detailed in Eq. 6. Consequently, the update magnitudes approach zero, resulting in diminished performance during fine-tuning on new tasks. To address this issue, we introduce a residual adapter $\mathbf{R}_{t+1}$ (initialized as $\mathbf{0}$) in parallel with $\mathbf{O}_{t+1}^v$, providing additional capacity for new tasks and maintaining a balance between stability and plasticity.

When the model is fine-tuned on the $(t+1)$-th task, the residual adapter $\mathbf{R}_{t+1}$ is updated within the subspace $\mathcal{R}_t$ (we set $\mathcal{R}_1 = \emptyset$) defined as

$$\mathcal{R}_t := \mathcal{V}_t \setminus \mathcal{V}_{t-1} \subseteq \mathbb{R}^d, \tag{7}$$

where $\mathcal{V}_t$ and $\mathcal{V}_{t-1}$ are the feature subspaces containing all bases of $\mathbf{\Phi}_t^v$ and $\mathbf{\Phi}_{t-1}^v$ obtained after fine-tuning on the t and $t-1$ tasks. It is worth noting that subspace $\mathcal{R}_t$ and $\mathcal{R}_{t+1}$ are specific to their corresponding tasks t and $t+1$, respectively, as $\mathcal{R}_{t+1} \cap \mathcal{R}_t = \emptyset$. Specifically, the subspace $\mathcal{R}_t$ indicates the residual knowledge extracted from the most recent task, providing supplementary bases to enlarge the optimization subspace.

Suppose the feature subspace $\mathcal{R}_t$ can be represented by the matrix $\mathbf{\Psi}_t \in \mathbb{R}^{r_t\times d}$. With these extracted bases, we are able to project the updates $\Delta\mathbf{R}_{t+1}$ into the subspace $\mathcal{R}_t$ by

$$\Delta\mathbf{R}_{t+1} \leftarrow \mathbf{\Psi}_t^T\mathbf{\Psi}_t\Delta\mathbf{R}_{t+1}. \tag{8}$$

When we conduct **fine-tuning** on the $(t+1)$-task, the value matrix $\mathbf{V}^{(l)}$ in the l-th layer given activations $\mathbf{h}^{(l)}$ can be found as

$$\mathbf{V}^{(l)} = \mathbf{a}^{(l)}\left(\mathbf{W}_0^v + \mathbf{O}_{t+1}^v\right) + \mathbf{a}^{(l)}\mathbf{R}_{t+1} = \mathbf{V}_o^{(l)} + \mathbf{V}_r^{(l)}, \tag{9}$$

where $\mathbf{W}_0^v$ is the pre-trained weights, and $\mathbf{V}_o^{(l)} = \mathbf{a}^{(l)}\left(\mathbf{W}_0^v + \mathbf{O}_{t+1}^v\right)$, $\mathbf{V}_r^{(l)} := \mathbf{a}^{(l)}\mathbf{R}_{t+1}$.

4.3. Dynamic Memory

As previously mentioned, the residual adapter $\mathbf{R}_{t+1}$ is updated within the subspace $\mathcal{R}_t$, a subset of the feature subspace $\mathcal{V}_t$ extracted from the t-th task. Consequently, the fine-tuning process may deteriorates the performance on prior tasks. To mitigate this issue, we introduce a *dynamic memory* mechanism that adjusts $\mathbf{V}_r^{(l)}$, the output of $\mathbf{R}_{t+1}$, during **inference** on test data as follows:

$$\hat{\mathbf{V}}^{(l)} = \mathbf{V}_o^{(l)} + \mathbf{a}^{(l)}\mathbf{\Omega}_{t+1}^T\mathbf{\Omega}_{t+1}\mathbf{R}_{t+1} = \mathbf{V}_o^{(l)} + \hat{\mathbf{V}}_r^{(l)}, \tag{10}$$

where $\mathbf{\Omega}_{t+1}^T\mathbf{\Omega}_{t+1}$ is computed according to the input activation signal $\mathbf{a}^{(l)}$. Specifically, the attention score $\mathbf{S}^{(l)} \propto \text{softmax}(\frac{\mathbf{Q}^{(l)}(\mathbf{K}^{(l)})^T}{\sqrt{d}})$, computed by applying $\mathbf{a}^{(l)}$ to the query and key weight matrices, reflects the relevance between the input test sample and the task associated with the extracted bases used to update the residual adapter $\mathbf{R}_{t+1}$. We utilize the matrices $\mathbf{\Psi}_\tau \in \mathbb{R}^{r_\tau\times d}$ $(\tau \le t+1)$, stored in memory, to multiply the first row of the attention score, $\mathbf{v}^{(l)} := \mathbf{S}_1^{(l)}$, as follows:

$$\text{if } r_\tau \neq 0, \omega_\tau = \frac{\left\|\mathbf{\Psi}_\tau \cdot \mathbf{v}^{(l)}\right\|}{r_\tau\left\|\mathbf{v}^{(l)}\right\|}, \text{ otherwise, } \omega_\tau = 0, \tag{11}$$

where r_τ indicates the rank of $\mathbf{\Psi}_\tau$. Since the task-specific residual bases remain independent across different tasks, the cosine similarity between feature vectors $\mathbf{v}^{(l)}$ extracted from input test samples and the stored core bases $\mathbf{\Psi}_\tau$ for each task can be used as a scaling factor for the corresponding components in the outputs of the residual adapter. This method assigns lower weights to components irrelevant to the current test samples, while components with high

Table 1. Metrics (%) computed from experiments on ImageNet-R. We report the average accuracy over 3 trials, each with different random seeds. The numeric after "±" denotes standard deviation.

Method	5-Split ImageNet-R		10-Split ImageNet-R		20-Split ImageNet-R	
	ACC(↑)	FT(↓)	ACC(↑)	FT(↓)	ACC(↑)	FT(↓)
LoRA	72.33 ±0.94	12.1 ±1.19	61.85 ±0.52	26.0 ±1.35	48.59 ±0.39	34.4 ±0.57
L2P	61.60 ±0.43	5.36 ±0.27	59.21 ±0.68	7.59 ±0.78	56.36 ±0.83	10.3 ±0.72
DualPrompt	68.47 ±0.23	3.18 ±0.24	66.72 ±0.30	4.15 ±0.11	64.40 ±0.18	5.82 ±0.51
PGP	69.07 ±0.28	3.41 ±0.18	64.22 ±4.53	4.23 ±0.22	64.19 ±0.38	6.50 ±0.31
S-Prompt	51.33 ±0.22	27.6 ±1.18	49.80 ±0.16	29.2 ±0.93	55.64 ±0.53	22.3 ±1.85
CodaPrompt	74.91 ±0.30	1.85 ±0.07	73.83 ±0.29	2.56 ±0.31	68.96 ±0.46	**3.25** ±0.40
InfLoRA	77.30 ±0.49	3.05 ±0.44	74.03 ±0.30	6.18 ±0.25	69.77 ±0.31	7.98 ±0.40
DualLoRA	78.55 ±0.12	2.61 ±0.25	76.23 ±0.33	3.67 ±0.66	71.25 ±0.31	5.45 ±0.27
DualLoRA+	**79.88** ±0.50	**1.10** ±0.16	**81.17** ±0.23	**2.04** ±0.05	**74.73** ±0.40	3.75 ±0.10

relevance to the samples are given proportionally higher weights. The resulting matrix, $\mathbf{\Omega}_{t+1}$, is obtained by:

$$\mathbf{\Omega}_{t+1} = \begin{bmatrix} \mathbf{\Sigma}_1 & \mathbf{0} & \cdots & \mathbf{0} \\ \mathbf{0} & \mathbf{\Sigma}_2 & & \\ \vdots & & \ddots & \vdots \\ \mathbf{0} & \mathbf{0} & \cdots & \mathbf{\Sigma}_{t+1} \end{bmatrix} \begin{bmatrix} \mathbf{\Psi}_1 \\ \mathbf{\Psi}_2 \\ \vdots \\ \mathbf{\Psi}_{t+1} \end{bmatrix} \in \mathbb{R}^{r' \times d}, \tag{12}$$

where $r' = \sum_{\tau=1}^{t+1} r_\tau$, $\mathbf{\Sigma}_\tau \in \mathbb{R}^{r_\tau \times r_\tau}$ is a diagonal matrix with the identical value $\omega_\tau^{1/2}$.

4.4. Task identity Prediction with Confidence

As the number of fully connected layers $f_t(\cdot)$ increases with the addition of tasks during continual learning, there is a risk that an irrelevant fully connected layer may generate the maximal logit, resulting in incorrect predictions for input test samples. This motivates us to propose a task identity prediction scheme based on task relevance, computed using $\mathbf{\Psi}_\tau$ as previously discussed.

As discussed in section 4.1, we sample m training data points to extract core bases after completing the t-th task. During this process, we obtain the average feature vector $\bar{\mathbf{v}}^{(L)}$ forwarded to the **final** attention block from each task and compute the similarity vector $\boldsymbol{\pi}_t = \{\omega_\tau\}_{\tau=1}^t$ based on Eq. 11. Therefore, we obtain a set $\mathbf{\Pi}_t = \{\boldsymbol{\pi}_1, \ldots, \boldsymbol{\pi}_t\}$ that can be used to distinguish the task identity during inference. Specifically, let $\boldsymbol{\pi}^\star$ denote the similarity vector computed from the input test sample, then we can predict the **task identity** by

$$\hat{k} = \arg\max_\tau g(\boldsymbol{\pi}_\tau, \boldsymbol{\pi}^\star) := \frac{\|\boldsymbol{\pi}_\tau \cdot \boldsymbol{\pi}^\star\|}{\|\boldsymbol{\pi}_\tau\| \cdot \|\boldsymbol{\pi}^\star\|}, \tag{13}$$

$$\hat{\delta} = \lambda \left(g(\boldsymbol{\pi}_{\hat{k}}, \boldsymbol{\pi}^\star) - \max_{\tau \neq \hat{k}} g(\boldsymbol{\pi}_\tau, \boldsymbol{\pi}^\star) \right), \tag{14}$$

where λ is a scaling factor, $\hat{k}$ denotes the predicted task identity and $\hat{\delta}$ indicates the confidence of this prediction. Moreover, we scale the output logits as

$$f_{\hat{k}}(\mathbf{h}^{(L)}) \leftarrow (1 + \hat{\delta}) \cdot f_{\hat{k}}(\mathbf{h}^{(L)}). \tag{15}$$

5. Experiments

5.1. Experimental Settings

Datasets and Metrics. We evaluate the proposed method DualLoRA on three continual learning benchmark datasets CIFAR100 [12], Tiny-ImageNet[13] and ImageNet-R[7]. To generate a sequence of tasks in a class-incremental setting as illustrated in Eq. 1, we randomly split the original dataset by class ID. This process creates multiple partitions, each containing an equal number of classes. Each partition corresponds to a distinct task. Following the strategy in existing studies in continual learning [21, 24, 28], we compute the final average accuracy (denoted by ACC) and degree of forgetting (denoted by FT) for evaluating the performance of our method and these two metrics can be found as

$$\text{ACC} = \frac{1}{T}\sum_{\tau=1}^{T} \text{acc}_{\tau,T}, \text{FT} = \frac{1}{T-1}\sum_{\tau=1}^{T-1} \text{acc}_{\tau,\text{best}} - \text{acc}_{\tau,T}, \tag{16}$$

where $\text{acc}_{\tau,T}$ denotes the accuracy of the τ-th task after the model learns the T-th task while $\text{acc}_{\tau,\text{best}}$ denotes the highest accuracy on the τ-th task during the whole fine-tuning process. Throughout the evaluation, we assume that the task identities of the testing data are **unknown**.

Baselines. Our baselines include vanilla LoRA, Learning To Prompt (L2P) [29], DualPrompt [28], Prompt Gradient Projection (PGP) [21], S-Prompt [27], CodaPromptprompt [24], and InfLoRA [17]. We focus on comparing the proposed DualLoRA with the state-of-the-art PEFT-based CL schemes since they are superior to traditional CL schemes. To demonstrate the **upper-bound** performance of DualLoRA, we implemented it under the setting where all samples in a batch share the same task identity, referred

Table 2. Metrics (%) computed from experiments on CIFAR100 and Tiny-ImageNet. We report the average accuracy over 3 trials, each with different random seeds. The numeric after "±" denotes standard deviation.

Method	10-Split CIFAR100		10-Split TinyImageNet		20-Split TinyImageNet	
	ACC(↑)	FT(↓)	ACC(↑)	FT(↓)	ACC(↑)	FT(↓)
LoRA	73.32 ±0.38	20.4 ±0.53	67.69 ±0.49	23.7 ±0.65	48.48 ±2.36	44.4 ±2.73
L2P	83.97 ±0.18	6.41 ±0.09	81.90 ±0.42	5.39 ±0.33	81.24 ±0.21	5.86 ±0.22
DualPrompt	85.85 ±0.22	5.41 ±0.12	85.10 ±0.10	3.95 ±0.22	82.77 ±0.12	5.31 ±0.10
PGP	85.28 ±0.01	5.60 ±0.34	84.83 ±0.21	4.32 ±0.16	83.49 ±0.35	5.24 ±0.31
S-Prompt	67.03 ±0.66	24.8 ±0.62	68.41 ±0.26	10.41±0.68	74.69 ±0.30	7.70 ±0.28
CodaPrompt	85.77 ±0.69	4.07 ±0.22	85.67 ±0.25	3.16 ±0.17	83.61 ±0.47	3.34±0.35
InfLoRA	85.62 ±0.74	4.34 ±0.06	81.28 ±0.40	8.62 ±0.36	75.89 ±0.38	13.8 ±0.11
DualLoRA	89.13 ±0.17	4.08 ±0.16	86.42 ±0.07	3.87 ±0.18	83.75 ±0.25	5.24 ±0.15
DualLoRA+	**90.94** ±0.15	**3.20** ±0.18	**87.74** ±0.21	**2.45** ±0.25	**84.65** ±0.07	3.61 ±0.13

to as **DualLoRA+**. In this scenario, we use average feature to compute similarity in the task identity prediction as described in Section 4.4 and facilitate more accurate task prediction, as the average feature exhibits less variance and is closer to the true mean.

Model Architecture and Hyperparameters. We use ViT-B/16 [4] backbone pretrained on ImageNet-21K as the foundation model throughout all experiments. We use the Adam optimizer [9] with parameters $\beta_1 = 0.9$ and $\beta_2 = 0.999$ for model fine-tuning, across 5 epochs with a batch size of 16 in all experiments. Unless specified, the rank of parameters in LoRA module is set to 10 in InfLoRA and DualLoRA. For a fair comparison, we set the specific hyperparameters leading to the best performance in each baseline, as shown in the original paper. More details of hyperparameters are provided in Appendix 2.

5.2. Experimental Results

ImageNet-R. As shown in Table 1, DualLoRA demonstrates comparable performance with InfLoRA, which outperforms other Prompt-based CL schemes in final average accuracy ACC. DualLoRA exhibits a slight performance decrease compared to InfLoRA by 1.25% on the 5-split benchmark, yet it outperforms InfLoRA by 2.2% and 1.48% on the 10-split and 20-split benchmarks, respectively. Forgetting serves as another metric to quantify the performance degradation on previous tasks, which may not consistently align with the average accuracy. CodaPrompt shows superior performance in mitigating forgetting, even though it does not achieve the same level as InfLoRA and DualLoRA in the average accuracy metric. DualLoRA+ significantly enhances both average accuracy and forgetting metrics, surpassing all other baselines except for securing the second position in the forgetting metric on the 20-split benchmark. DualLoRA+ outperforms the state-of-the-art scheme InfLoRA by 2.58%, 7.14%, and 4.96% in terms of

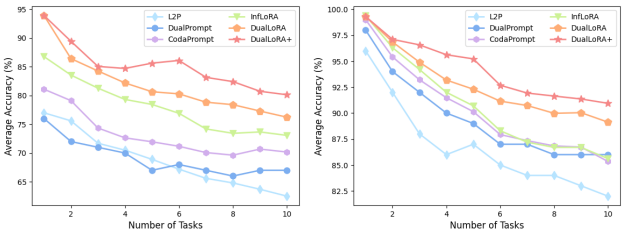

(a) ImageNet-R (b) CIFAR100

Figure 3. Figures (a) and (b) demonstrate the average accuracy of different methods during training.

average accuracy metric across the 5-split, 10-split, and 20-split settings. In addition, in terms of the forgetting metric, DualLoRA+ shows improvements over InfLoRA by 1.95%, 4.14%, and 3.23% respectively, in the same settings.

CIFAR100 and Tiny-ImageNet. DualLoRA steadily shows strong performance in these two datasets, achieving the best performance in average accuracy compared to prior existing schemes on CIFAR100 and Tiny-ImageNet benchmarks while slightly underperforming CodaPrompt on Tiny-ImageNet in forgetting metrics. DualLoRA+ consistently demonstrates extraordinary performance in average accuracy, outperforming CodaPrompt (the best schemes in these baselines) by 5.17%, 2.07% and 1.04%, respectively, and also demonstrating an advantage in the forgetting metric on 10-split CIFAR100 and 10-split Tiny-ImageNet. To give more insights, we report the average accuracy computed with different numbers of learned tasks, as illustrated in Fig. 3.(a) and 3.(b). As shown in the figures, DualLoRA and DualLoRA+ outperform other baselines in different stages of the continual learning. Furthermore, DualLoRA+ demonstrates robust resistance to forgetting as the number of learned tasks increases, suggesting the potential of DualLoRA+ fine-tuning foundational models across a wider range of tasks without significant forgetting.

Table 3. **O** stands for orthogonal adapter, **R** stands for residual adapter, and **Task ID** stands for giving true task ID during inference.

Method	10-Split ImageNet-R		10-Split CIFAR100		10-Split TinyImageNet	
	ACC(↑)	FT(↓)	ACC(↑)	FT(↓)	ACC(↑)	FT(↓)
LoRA	61.85	26.0	73.03	20.26	67.69	23.70
LoRA + O	74.11	4.65	84.03	5.67	83.92	7.74
LoRA + O + R	74.60	4.12	86.65	3.96	85.61	4.30
DualLoRA	76.23	3.67	89.13	5.08	86.42	3.87
DualLoRA+	81.17	2.04	90.94	3.20	87.74	2.45
DualLoRA + Task ID	87.66	0.46	94.39	1.05	95.71	0.84

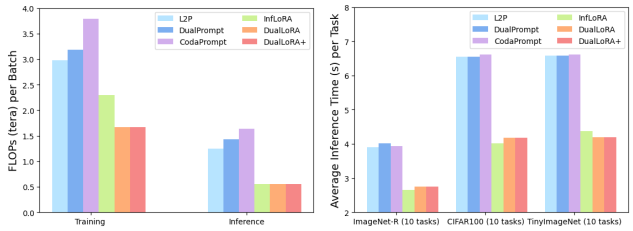

(a) FLOPs (b) Inference Time

Figure 4. Figure (a) demonstrates the approximated average FLOPs (Tera) during training and inference on each batch of data points. Figure (b) demonstrates the actual average running time for different schemes to perform inference on a task, using one NVIDIA A100 GPU.

5.3. Ablation Study

We perform additional experiments to confirm the effectiveness of various subroutines within the DualLoRA scheme. To be specific, we implement three variants of DualLoRA: (1) **LoRA + O** stands for only using the orthogonal adapter; (2) **LoRA + O + R** stands for running DualLoRA without performing task identity prediction; (3) **LoRA + O + R + Task ID** assumes knowing true task identities. As illustrated in Table. 3, the orthogonal adapter significantly improves the performance of LoRA while the residual adapter further enhances both average accuracy and forgetting metrics. Moreover, DualLoRA and DualLoRA+ further improve the performance by using individual features and average features to perform task identity prediction. The final configuration, where true task identities are utilized, exhibits superior performance in both average accuracy and forgetting, highlighting the crucial role of task prediction.

5.4. Computation and Inference Time

To better compare DualLoRA with other baselines in terms of computation, we report number of floating point operations (FLOPs) during the training and inference phases in Figure.4.(a) and the average inference time on a task in Figure.4.(b). According to the results in the figure, InfLoRA has the lowest FLOPs during inference, while DualLoRA has the lowest FLOPs during training because InfLoRA requires a double forward pass as mentioned earlier. During inference, InfLoRA and DualLoRA have similar inference time across different datasets, which are less than 50% inference time compared to the prompt-base CL schemes. Details on computing FLOPs are provided in Appendix 3.

5.5. Varying the Pre-Trained Models

To explore the consistency of DualLoRA's performance, we conduct experiments using the ViT-B/16 model pretrained on ImageNet-1k with both supervised learning and the unsupervised SAM framework [10]. As shown in the table, all schemes exhibit performance degradation when using a ViT model pretrained on unsupervised datasets. Nevertheless, DualLoRA consistently outperforms other schemes in terms of average accuracy.

6. Conclusion

We introduce DualLoRA, an innovative low-rank adaptation scheme for Vision Transformers (ViTs) that integrates orthogonal and residual adapters, operating in parallel with pre-trained weights. This structure achieves a balance between stability and plasticity in continual learning through a dynamic memory mechanism that leverages subspaces from previously learned tasks. Extensive experiments demonstrate that DualLoRA outperforms state-of-the-art continual learning methods across multiple benchmarks while requiring fewer computational resources. We see this work as an important step toward developing more efficient and effective continual learning paradigms for foundational models.

References

[1] Pietro Buzzega, Matteo Boschini, Angelo Porrello, Davide Abati, and Simone Calderara. Dark experience for general continual learning: a strong, simple baseline. *Advances in neural information processing systems*, 33:15920–15930, 2020. 1

[2] Hyuntak Cha, Jaeho Lee, and Jinwoo Shin. Co2l: Contrastive continual learning. In *Proceedings of the IEEE/CVF International conference on computer vision*, pages 9516–9525, 2021. 1

Table 4. Metrics computed from experiments on ImageNet-R (10 tasks) using varying pretrained ViTs. $\overline{\textbf{ACC}}$ denotes the average of **ACC** in every timestep.

	Method	ACC(%)	$\overline{\text{ACC}}$(%)
ImageNet-1k	L2P	60.23	67.86
	DualPrompt	67.45	72.48
	CodaPrompt	73.26	79.49
	InfLoRA	75.58	81.92
	DualLoRA	**77.28**	**82.63**
SAM-1k	L2P	52.71	58.24
	DualPrompt	56.57	63.23
	CodaPrompt	61.13	70.79
	InfLoRA	64.62	73.66
	DualLoRA	**66.44**	**74.70**

[3] Danruo Deng, Guangyong Chen, Jianye Hao, Qiong Wang, and Pheng-Ann Heng. Flattening sharpness for dynamic gradient projection memory benefits continual learning. *Advances in Neural Information Processing Systems*, 34: 18710–18721, 2021. 2, 4

[4] Alexey Dosovitskiy, Lucas Beyer, Alexander Kolesnikov, Dirk Weissenborn, Xiaohua Zhai, Thomas Unterthiner, Mostafa Dehghani, Matthias Minderer, Georg Heigold, Sylvain Gelly, et al. An image is worth 16x16 words: Transformers for image recognition at scale. *arXiv preprint arXiv:2010.11929*, 2020. 3, 4, 7

[5] Mehrdad Farajtabar, Navid Azizan, Alex Mott, and Ang Li. Orthogonal gradient descent for continual learning. In *International Conference on Artificial Intelligence and Statistics*, pages 3762–3773. PMLR, 2020. 2

[6] Qiankun Gao, Chen Zhao, Yifan Sun, Teng Xi, Gang Zhang, Bernard Ghanem, and Jian Zhang. A unified continual learning framework with general parameter-efficient tuning. In *Proceedings of the IEEE/CVF International Conference on Computer Vision*, pages 11483–11493, 2023. 4

[7] Dan Hendrycks, Steven Basart, Norman Mu, Saurav Kadavath, Frank Wang, Evan Dorundo, Rahul Desai, Tyler Zhu, Samyak Parajuli, Mike Guo, et al. The many faces of robustness: A critical analysis of out-of-distribution generalization. In *Proceedings of the IEEE/CVF international conference on computer vision*, pages 8340–8349, 2021. 6

[8] Edward J Hu, Yelong Shen, Phillip Wallis, Zeyuan Allen-Zhu, Yuanzhi Li, Shean Wang, Lu Wang, and Weizhu Chen. Lora: Low-rank adaptation of large language models. *arXiv preprint arXiv:2106.09685*, 2021. 1, 2, 4

[9] Diederik P Kingma and Jimmy Ba. Adam: A method for stochastic optimization. *arXiv preprint arXiv:1412.6980*, 2014. 7

[10] Alexander Kirillov, Eric Mintun, Nikhila Ravi, Hanzi Mao, Chloe Rolland, Laura Gustafson, Tete Xiao, Spencer Whitehead, Alexander C Berg, Wan-Yen Lo, et al. Segment anything. In *Proceedings of the IEEE/CVF International Conference on Computer Vision*, pages 4015–4026, 2023. 8

[11] Yajing Kong, Liu Liu, Zhen Wang, and Dacheng Tao. Balancing stability and plasticity through advanced null space in continual learning. In *European Conference on Computer Vision*, pages 219–236. Springer, 2022. 2

[12] Alex Krizhevsky, Geoffrey Hinton, et al. Learning multiple layers of features from tiny images. 2009. 6

[13] Ya Le and Xuan Yang. Tiny imagenet visual recognition challenge. *CS 231N*, 7(7):3, 2015. 6

[14] Brian Lester, Rami Al-Rfou, and Noah Constant. The power of scale for parameter-efficient prompt tuning. *arXiv preprint arXiv:2104.08691*, 2021. 1, 3

[15] Xilai Li, Yingbo Zhou, Tianfu Wu, Richard Socher, and Caiming Xiong. Learn to grow: A continual structure learning framework for overcoming catastrophic forgetting. In *International conference on machine learning*, pages 3925–3934. PMLR, 2019. 1

[16] Yan-Shuo Liang and Wu-Jun Li. Adaptive plasticity improvement for continual learning. In *Proceedings of the IEEE/CVF Conference on Computer Vision and Pattern Recognition*, pages 7816–7825, 2023. 2

[17] Yan-Shuo Liang and Wu-Jun Li. Inflora: Interference-free low-rank adaptation for continual learning. *arXiv preprint arXiv:2404.00228*, 2024. 2, 3, 5, 6

[18] Sen Lin, Li Yang, Deliang Fan, and Junshan Zhang. Trgp: Trust region gradient projection for continual learning. *arXiv preprint arXiv:2202.02931*, 2022. 2, 4

[19] Noel Loo, Siddharth Swaroop, and Richard E Turner. Generalized variational continual learning. *arXiv preprint arXiv:2011.12328*, 2020. 1

[20] Arun Mallya and Svetlana Lazebnik. Packnet: Adding multiple tasks to a single network by iterative pruning. In *Proceedings of the IEEE conference on Computer Vision and Pattern Recognition*, pages 7765–7773, 2018. 1

[21] Jingyang Qiao, Xin Tan, Chengwei Chen, Yanyun Qu, Yong Peng, Yuan Xie, et al. Prompt gradient projection for continual learning. In *The Twelfth International Conference on Learning Representations*, 2023. 3, 6

[22] Gobinda Saha and Kaushik Roy. Continual learning with scaled gradient projection. In *Proceedings of the AAAI Conference on Artificial Intelligence*, pages 9677–9685, 2023. 2

[23] Gobinda Saha, Isha Garg, and Kaushik Roy. Gradient projection memory for continual learning. *arXiv preprint arXiv:2103.09762*, 2021. 2, 4, 5

[24] James Seale Smith, Leonid Karlinsky, Vyshnavi Gutta, Paola Cascante-Bonilla, Donghyun Kim, Assaf Arbelle, Rameswar Panda, Rogerio Feris, and Zsolt Kira. Coda-prompt: Continual decomposed attention-based prompting for rehearsal-free continual learning. In *Proceedings of the IEEE/CVF Conference on Computer Vision and Pattern Recognition*, pages 11909–11919, 2023. 2, 3, 6

[25] Liyuan Wang, Xingxing Zhang, Hang Su, and Jun Zhu. A comprehensive survey of continual learning: Theory, method and application. *IEEE Transactions on Pattern Analysis and Machine Intelligence*, 2024. 1

[26] Shipeng Wang, Xiaorong Li, Jian Sun, and Zongben Xu. Training networks in null space of feature covariance for continual learning. In *Proceedings of the IEEE/CVF conference on Computer Vision and Pattern Recognition*, pages 184–193, 2021. 2

[27] Yabin Wang, Zhiwu Huang, and Xiaopeng Hong. S-prompts learning with pre-trained transformers: An occam's razor for domain incremental learning. *Advances in Neural Information Processing Systems*, 35:5682–5695, 2022. 2, 3, 6

[28] Zifeng Wang, Zizhao Zhang, Sayna Ebrahimi, Ruoxi Sun, Han Zhang, Chen-Yu Lee, Xiaoqi Ren, Guolong Su, Vincent Perot, Jennifer Dy, et al. Dualprompt: Complementary prompting for rehearsal-free continual learning. In *European Conference on Computer Vision*, pages 631–648. Springer, 2022. 3, 6

[29] Zifeng Wang, Zizhao Zhang, Chen-Yu Lee, Han Zhang, Ruoxi Sun, Xiaoqi Ren, Guolong Su, Vincent Perot, Jennifer Dy, and Tomas Pfister. Learning to prompt for continual learning. In *Proceedings of the IEEE/CVF Conference on Computer Vision and Pattern Recognition*, pages 139–149, 2022. 2, 3, 6

[30] Martin Wistuba, Prabhu Teja Sivaprasad, Lukas Balles, and Giovanni Zappella. Continual learning with low rank adaptation. *arXiv preprint arXiv:2311.17601*, 2023. 2

[31] Yue Wu, Yinpeng Chen, Lijuan Wang, Yuancheng Ye, Zicheng Liu, Yandong Guo, and Yun Fu. Large scale incremental learning. In *Proceedings of the IEEE/CVF conference on computer vision and pattern recognition*, pages 374–382, 2019. 1

[32] Zhen Zhao, Zhizhong Zhang, Xin Tan, Jun Liu, Yanyun Qu, Yuan Xie, and Lizhuang Ma. Rethinking gradient projection continual learning: Stability/plasticity feature space decoupling. In *Proceedings of the IEEE/CVF Conference on Computer Vision and Pattern Recognition*, pages 3718–3727, 2023. 2, 4